18 Western North American Extreme Heat, Associated Large Scale Synoptic-Dynamics, and Performance by a Climate Model

Richard Grotjahn

18.1. Introduction

How well do we understand the dynamics and predictability of extreme heat events? This chapter will not answer such a broad question, but instead will focus on a context in which one can begin to address the question. Illustrative examples of some aspects of the dynamics and predictability will be shown for hot spells affecting much of western North America.

Various definitions and criteria abound for 'heat waves' (Table 1 in Grotjahn, 2011). In this report the more general term 'hot spells' is used to describe unusually hot maximum temperatures persisting a day or longer.

Generally speaking, North American extreme hot spells are associated with large scale displacements of air masses, placing unusually warm air where it is not normally found. Examples are numerous and occur over a wide range of time scales. A lengthy heat wave affected the central United States from June-August during the summer of 1980 (Karl and Quayle, 1981; Namias, 1982). An intermediate time scale event, 16-26 July 2006,affected California (and subsequently other regions of North America to the east and north Gershunov *et al.*, 2009) Events shorter than three days, more properly called hot spells, are also of interest though three days is a commonly-used minimum period (Grotjahn and Faure, 2008, Bumbaco *et al.*, 2013). In each case, the displacement of the hot air mass is reflected in the geopotential height fields and hence the winds. So the displacement results in a large scale pattern for several primary meteorological variables. These large scale meteorological patterns (LSMPs) will be a focus of this Chapter.

Monthly mean data are not adequate to resolve heat waves nor the associated LSMPs. As an illustration, one of the largest temperature anomalies in the past 60 years at California Central Valley (CV) stations occurred in early July, 1991. Temperature anomalies at the stations were more than 1.6 standard deviations above normal for four successive days. Most of the rest of the month was below average, so that the monthly mean for July 1991 was -0.2 standard deviations (i.e. below normal). Hence, a daily time scale is needed to resolve the LSMPs.

The remaining sections of this chapter discuss the synoptics and dynamics of the large scale meteorological patterns (LSMPs) associated with California extreme hot spells. Then the predictive ability of the LSMPs is shown in an illustrative pilot study. Finally, LSMPs are used in a simple assessment of both a model skill and future prediction of hot spells by the model.

18.2 California Heat waves: upper air large scale meteorological patterns (LSMPs) synoptics and dynamics

A synoptic description of the regional conditions conducive to a hot spell affecting much of central and northern California is shown in Figure 18.1. The figure shows composite averages of several representative variables, combining the times that 14 different extreme hot spells started. The hottest days occur when these conditions are met. First, temperatures need to be elevated in the upper atmosphere. The elevated temperatures (figure 18.1a) result in part from air advected from the Desert Southwest. Those elevated temperatures occur in part due to the parched source region and with strong sinking (figure 18.1b). Sinking is the normal state during summer over California and a subsidence inversion is a common occurrence. During the hottest days, the subsidence is stronger, and the inversion lower resulting in a thinner layer of near surface air for solar radiation to heat up. The geographic location of the anomalously high temperature values is crucial, with the hotter temperatures being at or off shore, causing the 'thermal low' in sea level pressure to migrate to the coast (figures 18.1a,c). The result is a near-surface pressure gradient that opposes the formation of a sea breeze (figure 18.1d). In addition, the flow has a downslope component above the western slope of the Sierra Nevada Mountains. (A shallow upslope flow can be created by solar radiative heating, but above the boundary layer the topography accentuates the sinking, adiabatic warming, and intensification downstream of the subsidence inversion over the Central Valley.) Further discussion of this figure is in Grotjahn (2011).

Figure 18.1 near here

A major contributing factor to an extreme heat wave can be drought. For example, the extreme European drought of 2003 was preceded by drought over a region including most of France and portions of adjacent countries. A major heat wave during March 2012 in the northern central part of the U.S. was amplified by extensive drought over the same region. Daily weather maps all show that the greatest heat anomaly occurred as hot air was drawn northward just east of the Rocky Mountains. Drought has less importance for California hot spells since the state experiences an annual drought during the summer months. Also, even when drought is ongoing, there are cooler and hotter periods but the latter still occur with the hot spells LSMPs.

Identification of the LSMPs begins with identification of relevant 'target' dates. Two different criteria are used to identify target dates. When discussing the onset and patterns leading up to the onset, the dates are the first day of a period lasting at least three days with maximum temperatures exceeding 38C and with at least one day greater than 40.5C at Sacramento California station KSAC. When discussing and using an 'LSMP index', the target dates are defined as when three CV stations are all exceeding their own normalized maximum temperature anomaly threshold of 1.6 standard deviations. The three stations are: KRBL, KFAT, KBFL. The value of 1.6 is exceeded by all three stations simultaneously about 1% of the time during the recent 30 year period (1979-2008).

Meteorological fields on the target dates are composited to form the LSMPs, when either set of criteria is applied. The fields may be total fields or anomaly (with respect to long term means) fields. The LSMPs

are thus a 'target' ensemble mean constructed from a specified number of target dates. For example, the LSMP index is constructed based on the target ensemble mean of 16 dates that occurred during 1979-88. The target ensemble mean is further evaluated by comparing it against a large number of 'random' ensemble means, using the same number of dates each time, but where the dates are selected randomly, with replacement, from the historical record. The number of random ensemble means drawn is 1000. When the value at a grid point in the target ensemble mean equals or exceeds the highest 10 values at that grid point amongst the random ensemble means, then the target ensemble is in the highest 1% of values at that point. This procedure, referred to as 'bootstrap resampling' provides a means to identify parts of the LSMP that are statistically significant and hence warrant attention. In figure 18.1, shading indicates the highest and lowest 1.5% of the values of the variable based on this methodology. In addition to significance, consistency amongst the target ensemble members must be assessed. Consistency tests include: low values of the variance between ensemble members (compared with members in each random ensemble) and simple sign counts at each grid point. The sign count is the number of ensemble members having the same sign anomaly with respect to the long term daily mean minus those ensemble members having the opposite sign.

Figure 18.2 near here

Figure 18.2a shows the target ensemble mean 850hPa temperature anomaly field; this field can be compared with the total field (for a smaller region) shown in figure 18.1a. The other parts of figure 18.2 show the 16 individual target ensemble members. The upper air data used are from the National Centers for Environmental Prediction / Department of Energy reanalysis (hereafter, NDRA2) described in Kanamitsu *et al.* (2002). Shading in figure 18.2 indicates the anomaly value (not significance). Darker shading indicates higher anomaly value while lighter shading surrounded by a very dark ring indicates the lowest (largest negative) values. The figure is discussed further in Grotjahn (2011). The progressively darker shading indicates progressively higher (positive) values. The pattern is very consistent in having a strong positive anomaly at and just off the northern California coast. While there are often negative extrema West and East of the positive anomaly, the location and intensity of those negative extrema are inconsistent between the ensemble members.

Figure 18.3 near here

Figure 18.3 shows the ensemble average 500 hPa geopotential height daily anomaly field at the onset and at several times prior to the onset. This time evolution shows that the expected strong ridge centered near the west coast of North America is preceded by unusually high geopotential height values in the southeastern United States and northwestern Pacific. The strong ridge in the northwest Pacific precedes a trough in the east-central Pacific that in turn builds the ridge along the North American west coast. While that occurs, the ridge in the Southeastern U.S. diminishes or possibly migrates westward. This chain of events can be seen in a simple Hovmöller diagram (figure 18.4). Bumbaco *et al.* (2013) also find an upstream trough for heat waves affecting latitudes north of the CV (western Washington and Oregon).

Figure 18.4 near here

Figure 18.5 shows some dynamical analysis of the LSMPs using ensemble mean data. In figure 18.5a, contours of low frequency (periods longer than 14 days) 850 hPa temperature are shown with vectors of high frequency (periods less than 7 days) heat flux one day prior to the onset of 23 different hot spells. The eddy heat flux is advecting a 'bubble' of higher temperature air in a direction northwestward: along and just offshore of Northern California and Oregon.

Figure 18.5 near here

The large ridge along the west coast present during hot spells suggests drawing a parallel to the dynamics of blocking studies, though the season is summer, not winter. In figure 18.5b, the horizontal components of $E_u = \{ \frac{1}{2} [(v')^2-(u')^2], -u'v' \}$ are plotted along with the low frequency zonal wind component at 300 hPa. In E_u the high frequency (periods less than 7 days) zonal wind is u' while v' is the corresponding meridional component. The figure shows the composite of 23 events at their onset. Trenberth (1986) shows that the divergence of E_u is proportional to the total derivative of the zonal wind component. The figure shows convergence of the vectors off the west coast, indicative of slowing the zonal wind thereby building the ridge. In a related analysis, the dot product of the high frequency E vector with the gradient of the low frequency zonal wind is proportional to the barotopic energy conversion for a mass of the atmosphere. (See further discussion in Dole and Black, 1990; Black and Evans, 1998) In this analysis, $E = \{ [(v')^2-(u')^2], -u'v' \}$. On the North side of jet stream axis, that dot product is negative, implying that the high frequency eddy loses energy to the low frequency flow. On the west side of the ridge, the low frequency flow also gains energy, but the prior analysis showed the zonal component to be diminishing, hence the meridional component must be increasing. In short, the ridge is being amplified.

18.3 LSMPs as a predictor of surface extreme heat

A simple index can be formulated to measure how similar a particular day is to days when extreme hot spells occur. This index is a combination of un-normalized projections: one for each given daily anomaly field projected onto the corresponding field from the target ensemble of hottest days. Each projection is only calculated for one or more regions of the LSMP where that variable has significant amplitude and high consistency in the LSMP. The combination results in one number for each day, which is called the 'LSMP index' in this document. Further details are found in Grotjahn (2011, who calls this a 'circulation index'). Grotjahn (2011) has an illustrative pilot calculation using only 2 variables: temperature at 850 hPa and meridional wind at 700 hPa. Those choices are not ideal but were dictated by available data for a climate model application at that time. The relative weighting of the 2 projections to form the LSMP index was based on best capturing of the extreme events during the 1979-88 training period.

The properties of this LSMP index are discussed at length in Grotjahn (2011). A brief summary is presented here to provide a context for applying this approach to analyze climate model output in the next section.

Higher LSMP index values imply hotter surface temperatures. The LSMP index is intended to capture the extreme hottest days. Almost half of the dates match when comparing the highest 1% of the index values versus the hottest 1% of the Central Valley surface temperatures. Most of the other highest values of the index occur on days that are among the hottest 2% of the observed surface temperatures. The index also has a few of its highest 1% values during days that are merely above normal. The index has considerable

skill in capturing extreme events compared to chance using various measures of skill in forecasting rare events.

The LSMP index also does a good job of identifying days that are near normal and even below normal. (The meteorological patterns for unusually cool days enhance the sea breeze with an upper level trough, essentially the inverse of hot spell LSMPs.) So the observed upper air LSMP index and surface max temperatures are highly correlated. (Correlation equals 0.83 during verification period: 1989-2006) (To illustrate, figure 4 in Grotjahn, 2011, compares the LSMP index and the observed maximum surface temperature anomalies for the 10 year training period and the subsequent 18 year testing period.) Given the high correlation, one might expect the simulation of the LSMP index distribution to be a good indicator of how well the model could simulate surface temperatures.

Of course the LSMP index is just an approximation to how conducive the large scale conditions are to a hot spell. The index does not incorporate other relevant factors like those that reduce the heat (irrigation) and those that enhance the heat (drought and urbanization). With those caveats, distributions of the circulation indices for reanalysis, corresponding model data and for two future scenarios are shown next.

18.4 How well are LSMPs captured by a climate model?

This section makes an analysis of the LSMPs present in the fourth generation NCAR Community Climate model (CCSM4). The specific version uses 1.1 degree finite volume resolution. See Gent *et al*. (2011).One reason for examining the model LSMPs is because surface maximum temperatures can be poorly simulated in the climate model due to insufficient topographic resolution, poor surface and boundary layer simulation during the extremes, incorrect soil moisture, and inadequate surface type (vegetation/urban). Another reason is that the LSMPs are essentially the boundary conditions needed by a regional climate model that is better able to simulate regional climate. Hence, if the global model does not produce the LSMPs adequately enough, then even a superb regional model cannot properly simulate the hot spell.

The topography of California is very complex. CCSM4 at ~1.1 degree resolution cannot capture this complexity. Instead of a rather flat, low elevation CV ringed by higher mountain ranges with a few low passes accessing the ocean, the model has a broad gentle slope. (See fig. 1 in Grotjahn, 2013.) One consequence is the CCSM4 grid points near the CV stations are several hundred metres higher than the actual stations.

When maximum observed daily surface temperatures (an average of 3 stations that span the CV) are compared with the corresponding average of CCSM4 grid points close to those station locations, the model values are ~6K cooler than the observed maxima. (The averages are over a 55 year period.) One might assume this bias is due to the higher elevations of the CCSM4 surface but that would require a super-adiabatic lapse rate. Furthermore, the actual CV stations are placed in a heavily irrigated domain (which lowers the observed temperatures on the order 3K) and the climate model knows nothing about that irrigation. The standard deviation in the observed data versus the model data (4.38C versus 4.7K) and the skew (-0.31 vs -0.27) do match well. However, the distribution of model maximum surface temperature cannot be simply fixed by a simple shift of the whole distribution.

Figure 18.6 near here

A trivial addition of 6K to the model temperatures is inadequate as a bias correction procedure because the model hot spells LSMP is flawed. Figure 18.6 compares ensemble mean daily anomaly fields, where the ensemble is constructed from the hottest 1% of observed days (reanalysis data on top row) and hottest 1% of simulated surface temperatures near the California Central valley (CCSM4 data on bottom row). The general structures look similar, but that is hardly surprising. In both ensembles the model and observations have high temperatures through a depth of the lower troposphere and the mid-tropospheric winds are mainly geostrophic. More interesting is that the model has weaker amplitude in its LSMP. Hence, this model, even as a driver of a regional model, will not produce extreme hot spells. And it will not produce extremes often enough (Grotjahn, 2013). Even more interesting is that the model data have the maximum thermal anomaly over the CV grid points, but the observation-based reanalysis data have that maximum offshore (primarily to suppress the sea breeze). Hence, the model is completely missing this regional process.

If scatter plots are made of the LSMP index versus the surface maximum temperatures, then the general skill of the LSMP index as a predictor of surface maximum temperatures can be visualized. Such plots are found in Grotjahn (2013) but not reproduced here. The higher elevation of the CCSM4 surface makes the LSMP index less independent of the surface values, even though the fields used in the LSMP index occur 12 hours before the maximum temperature.

Figure 18.7 near here

CCSM4 has less variability in the LSMP index than does the reanalysis data as can be seen in figure 18.7. The standard deviation is 0.9 in the reanalysis data, but less than 0.8 in the model data. The skew is too little in the model (-0.11) versus the reanalysis data (-0.16). Even so, the CCSM4 data have fewer events above a given threshold that occurs rarely in the observations (reanalysis data). For example, using a the threshold of 2.0 corresponds to the top ~2% of the LSMP index for the reanalysis data (1951-2005) but the corresponding index for CCSM4 data have fewer than half as many members (50 instead of 111). These model biases hold for sub periods as well, with one exception, the model has a slight trend of increasing values that is *not* seen in the reanalysis LSMP index values. Grotjahn (2013) found a similar under-prediction of events though the average duration (~2.5 days) agreed well with reanalysis data.

Figure 18.8 near here

Keeping in mind these biases, one can consider how the model simulates California hot spells LSMPs in future climate. Figure 18.8 shows how the distribution of LSMP index in CCSM4 evolves for two representative concentration pathways (RCPs). The RCPs are defined in Moss *et al*. (2008). Both RCP scenarios show a shift to higher LSMP index values: about half a standard deviation for RCP4.5 and nearly a full standard deviation higher for RCP8.5. The magnitude of the skew is generally larger than in the historical simulations by this model. Hence, the mean and median are shifting more than the extreme values. Curiously, in the lower emission scenario the distributions are shifted but, the interdecadal variation does not show a continuing shift, and possibly a decline in the bulk of the index values. In contrast, for the higher emission scenario, each later distribution has a clear shift of the whole pattern to a higher value. These changes have implications for the durations of extremes and raise some questions.

The shift in future scenarios of the distributions relative to the recent historical period (figure 18.8) makes it more likely that more days will be above one standard deviation. Consequently, durations above some threshold are much more common and last much longer. For example, durations above 1 standard deviation are shown in figure 18.9. In the historical period, only 4 periods last longer than 9 days. For the lower emission case (RCP4.5) there are ~10 times as many (38) periods lasting longer than 9 days. A couple of periods each last more than 3 weeks. For the higher emission case (RCP8.5) there are 25 times as many (100) periods lasting longer than 9 days (1569 out of 6710 days). Indeed, the number of periods peaks at 4-5 days for RCP 8.5, confirming that this is the new normal implied by this scenario. Two of the periods are above 1 standard deviation for more than a month!

Figure 18.9 near here

There are commensurate changes in the LSMP index value corresponding to a 20-year return value. During 1951-2005, the 20-year return value is 2.2. The corresponding return value for 2046-2100 increases to: 2.8 for the RCP 4.5 and 3.1 for the RCP 8.5 scenarios. These are 25% and 40% increases. The RCP 8.5 return value is outside the range of values estimated for the historical period.

It is unclear how much to trust CCSM4's picture of future hot spells. One can see some problems by visualizing all the LSMP index data as in figure 18.10. First, the smaller standard deviation of the CCSM4 data is quite apparent from the scatter of values during the 55 year historical period (figures 18.10a,b). When these data are fit to a regression line, another problem mentioned before is apparent: there is a trend in the CCSM4 data but it is much smaller in the reanalysis data. Since both sets of data are based on upper air quantities and the portions of those quantities used are located primarily over the Pacific Ocean, then neither the CCSM4 trend nor the lack of one in the reanalysis data can be explained by a lack (or presence) of Central Valley irrigation. There must be a dynamical difference between model and observations (reanalysis).

Figure 18.10 near here

The future climate scenarios (figures 18.8 and 18.10c,d) are a mixture of expected and unexpected results. There is a strong trend (increasing values over time) in the RCP8.5 data as one might expect. Oddly, for the RCP4.5 values there is a slight decreasing trend. The extreme values have corresponding trends: increasing for RCP8.5, decreasing for RCP4.5 during 2046-2099. Given that the model has a positive trend where none existed historically, does the decreasing trend of RCP4.5 imply a strongly decreasing trend of future LSMP index values? Such a question is beyond the scope of this chapter. Instead, these results raise deeper issues about the model's simulation skill in handling the dynamics of extreme hot spells.

18.5 Conclusions

This chapter examined California Central Valley (CV) hot spells from the perspective of the large scale meteorological patterns (LSMPs) associated with those events. The LSMPs are large in scale and

magnitude, and hence potentially well-resolved by climate models. Such LSMPs form the basis for statistical and dynamical downscaling.

The LSMPs are found by compositing the data on target days, where the target days are dates of hot spells or their onset. Bootstrap re-sampling, which compares the target ensemble mean to a large number of randomly-drawn ensemble means, is used to identify significant areas. In addition to significance, areas of consistent behavior amongst the target ensemble members are also needed. Some other statistical issues were described. Areas that are both significant and consistent in upper air data were used in an un-normalized projection scheme to obtain an index of how similar a given day is to the target ensemble mean. This upper air 'LSMP index' is generally positive and larger the hotter the daily maximum surface temperatures are. Though intended just for the positive extremes, the LSMP index also models well the whole distribution of daily maximum surface temperatures. CV cooler days have a somewhat opposite LSMP to the hot spells during summer. Hence, the LSMP index is highly correlated with all the daily summer maximum temperatures in the CV. Some simple dynamical and synoptic interpretations were applied to understand better the LSMPs.

An LSMP-based index was used to assess hot spells created by the NCAR climate model CCSM4. The LSMP index is used because: a) the model has no Central Valley in its topography, b) the model does not simulate surface temperatures adequately, and c) the index has relevance to downscaling methods. The model does resolve and capture the large scale patterns associated with hot spells. While similar, the model patterns during hot spells are not as strong as observed and have key differences partly related to the smooth model topography.

An LSMP index provides a compact way of describing a complex pattern associated with hot spells. As such, other analyses can be done using that index. Properties of the index were examined and implications for the future climate were drawn along with concerns about how well the model can capture extreme events. For historical periods CCSM4: a) has notably less variability in LSMP index than is observed, b) underestimates the extremes by about half, and c) has an increasing trend in LSMP index that was not observed. In future climate scenarios for the last half of this century, CCSM4: a) has a strong increasing trend in LSMP index for the higher emission (RCP8.5) scenario, but a peculiar, slight decreasing trend in the lower emission (RCP4.5) scenario, b) extreme values have corresponding trends, such that 20-year return values (not shown) exceed the historical asymptote, i.e. are unprecedented for RCP8.5, and c) extreme events have much longer duration than historically, becoming commonplace.

The biases and curious results of the CCSM4 LSMP index need some additional quantification. Dynamical tools can be applied to understand why these biases and curious results are occurring in the model. Given daily, instantaneous, upper air and surface data, this LSMP approach can be applied to other models and potentially to investigate hot spells occurring in other regions of the Earth. Finally, the LSMP approach is potentially applicable to other extreme events, particularly cold air outbreaks and heavy frontal cyclone precipitation (Grotjahn and Faure, 2008).

Acknowledgements. This research was supported in part by the United States National Science Foundation under Grant No. 1236681. Dr. Yun-Young Lee prepared the figure of 500 hPa height anomalies.

References

Black, R. X., and Evans, K. J. (1998) The statistics and horizontal structure of anomalous weather regimes in the Community Climate Model. *Monthly Weather Rev*iew, **126**, 841-859.

Bumbaco, K. A., Dello, K. D., and Bond, N. A. (2013) History of Pacific Northwest Heat Waves: Synoptic Pattern and Trends*. *Journal of Applied Meteorology and Climatology*, **52**, 1618–1631.doi: http://dx.doi.org/10.1175/JAMC-D-12-094.1

Dole, R. M., and Black, R. X. (1990) Life cycles of persistent anomalies. Part II: The development of persistent negative height anomalies over the North Pacific Ocean. *Monthly Weather Review,* **118,** 824–846.

Gent, P. R., Danabasoglu, G., Donner, L. J., Holland, M. M., Hunke, E. C., Jayne, S. R., Lawrence, D. M., Neale, R. B., Rasch, P. J., Vertenstein, M., Worley, P. H., Yang, Z.-L., and Zhang, M. (2011) The Community Climate System Model Version 4. *Journal of Climate*, **24**, 4973–4991. doi: http://dx.doi.org/10.1175/2011JCLI4083.1

Gershunov, A., Cayan, D.R., and Iacobellis, S.F. (2009) The great 2006 heat wave over California and Nevada: Signal of an increasing trend. *Journal of Climate***22**, 6181-6203.

Grotjahn, R. (2011) Identifying extreme hottest days from large scale upper air data: a pilot scheme to find California Central Valley summertime maximum surface temperatures. *Climate Dynamics* **37**, 587–604. DOI 10.1007/s00382-011-0999-z

Grotjahn, R., and Faure, G. (2008) Composite predictor maps of extraordinary weather events in the Sacramento, California, region. *Weather and Forecasting*, **23**, 313–335. doi: http://dx.doi.org/10.1175/2007WAF2006055.1

Kanamitsu M., Ebisuzaki, W., Woollen, J., Yang, S. K., Hnilo, J., Fiorino, M., and Potter, G. (2002) NCEP-DOE AMIP-II reanalysis (R-2). *Bulletin of the American Meteorological Soc*iety, **83**, 1631–1643.

Karl, T. R., and Quayle, R. G. (1981) The 1980 Summer Heat Wave and Drought in Historical Perspective. *Monthly Weather Review*, **109**, 2055–2073. doi: http://dx.doi.org/10.1175/1520-0493(1981)109<2055:TSHWAD>2.0.CO;2

Moss, R., Babiker, M., Brinkman, S., Calvo, E., Carter, T., Edmonds, J., Elgizouli, I., Emori, S., Erda, L., Hibbard, K., Jones, R.,Kainuma, M., Kelleher, J., Lamarque, J. F., Manning, M., Matthews, B.,Meehl, J., Meyer, L., Mitchell, J., Nakicenovic, N., O'Neill, B., Pichs, R.,Riahi, K., Rose, S., Runci, P., Stouffer, R., van Vuuren, D., Weyant, J., Wilbanks, T., van Ypersele, J. P., and Zurek, M. (2008) *Towards New Scenarios for Analysis of Emissions, Climate Change, Impacts, and Response Strategies*. Intergovernmental Panel on Climate Change, Geneva, 132 pp.

Namias, J. (1982) Anatomy of Great Plains Protracted Heat Waves (especially the 1980 U.S. summer drought). *Monthly Weather Review*, **110**, 824–838. doi: http://dx.doi.org/10.1175/1520-0493(1982)110<0824:AOGPPH>2.0.CO;2

Trenberth, K. E. (1986) An assessment of the impact of transient eddies on the zonal flow during a blocking episode using localized Eliassen-Palm flux diagnostics. *Journal of the Atmospheric Sciences*, **43**, 2070-2087.

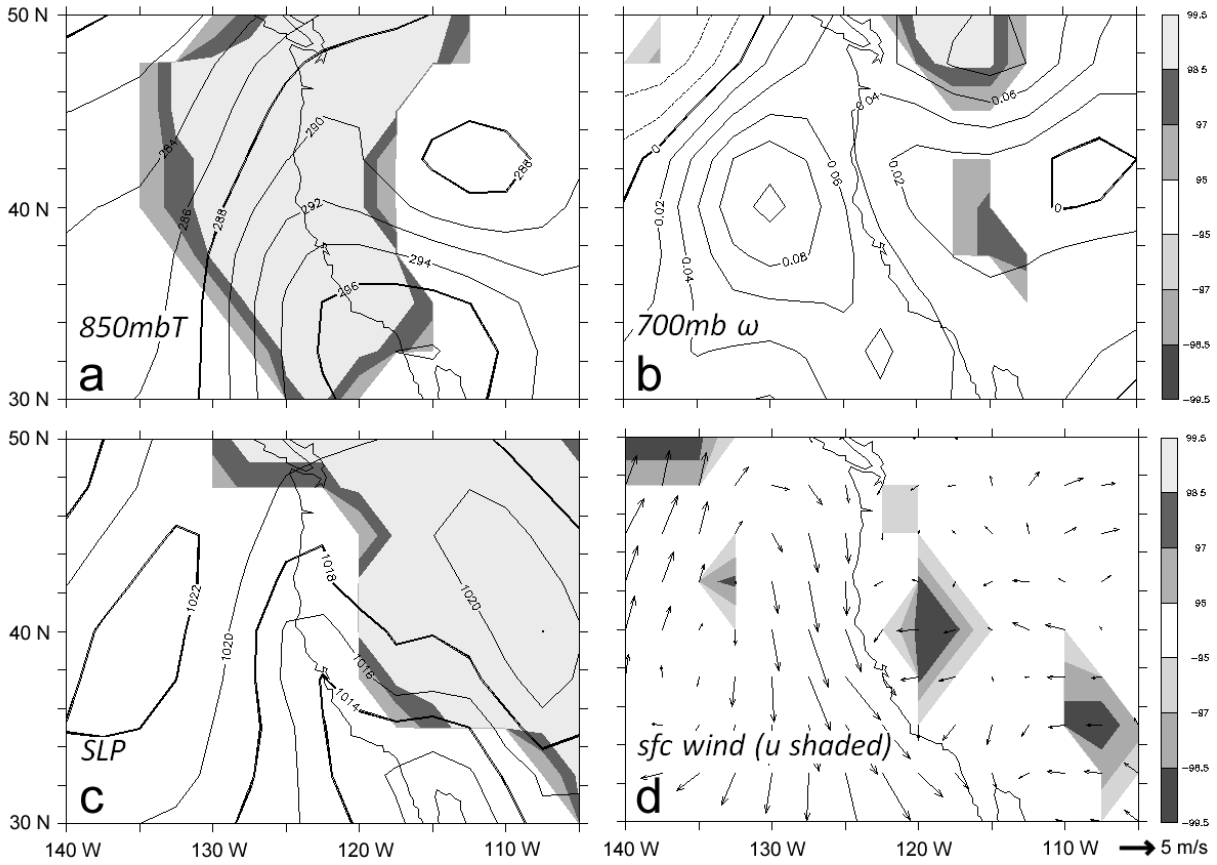

Figure 18.1 Synoptic conditions at the onset of a hot spell affecting the California Central Valley. Shown are ensemble averages of a) temperature at 850 hPa, b) pressure velocity at 700 hPa, c) sea level pressure, and d) surface wind vectors, where the shading applies to the zonal component. Shading indicates unusual values for the variables. Light shading surrounded by darker shading indicates composite values of the ensemble of extreme hot spell in the top 1.5% of a distribution of randomly-drawn composites. Darker shading surrounded by lighter indicates composite values in the lowest 1.5% of randomly-drawn composites.

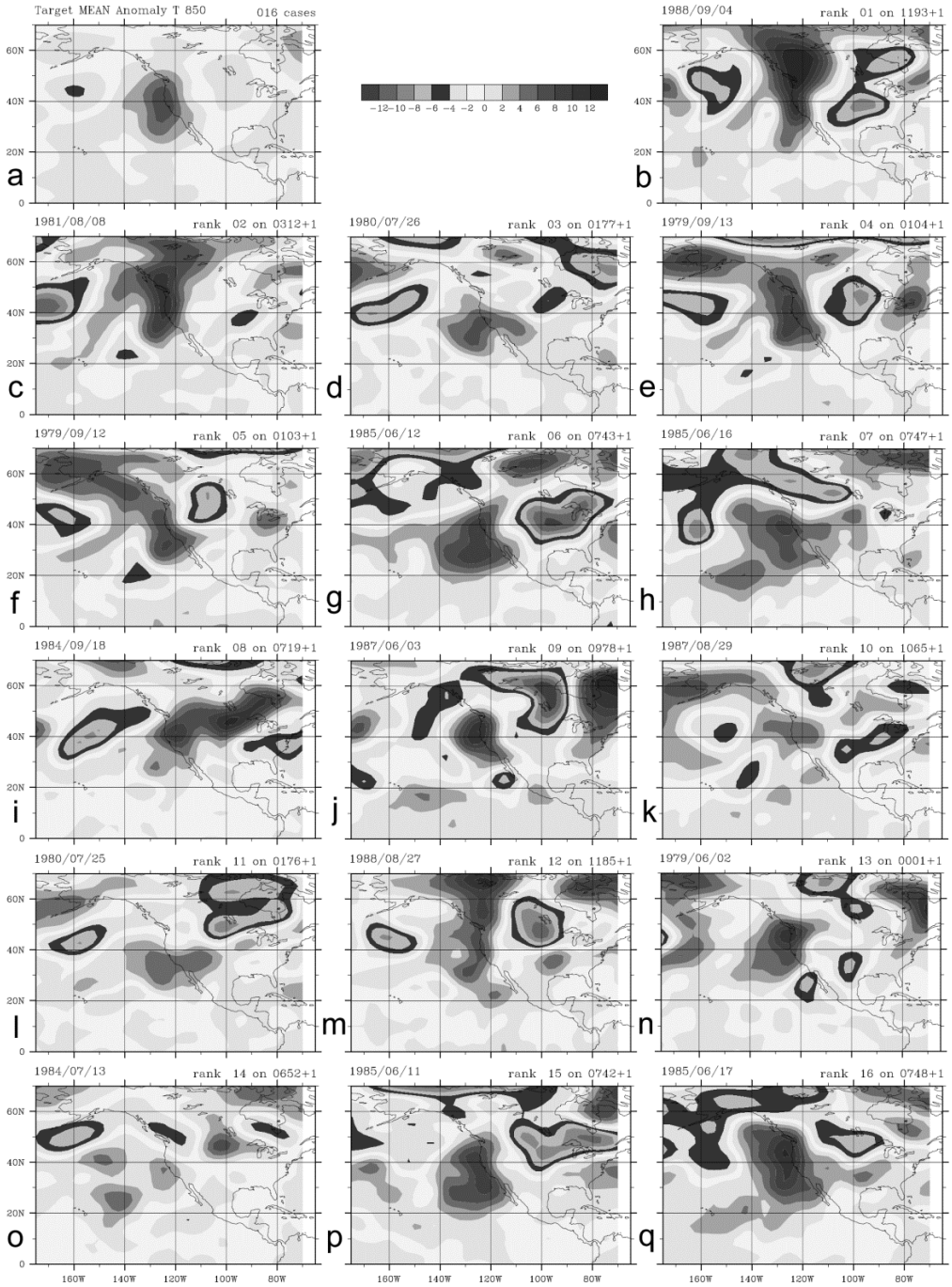

Figure 18.2Daily temperature anomalies at 850 hPa for the a) target ensemble mean and b) – q) members of the ensemble, one for each target date. The hottest event in the ensemble is b) and the least hot is q). There is a consistent location of strong, positive anomaly (light shading that becomes darker for higher anomaly values) at and just off shore of northern California. Negative anomalies are shaded in a way surrounded by a dark black ring.

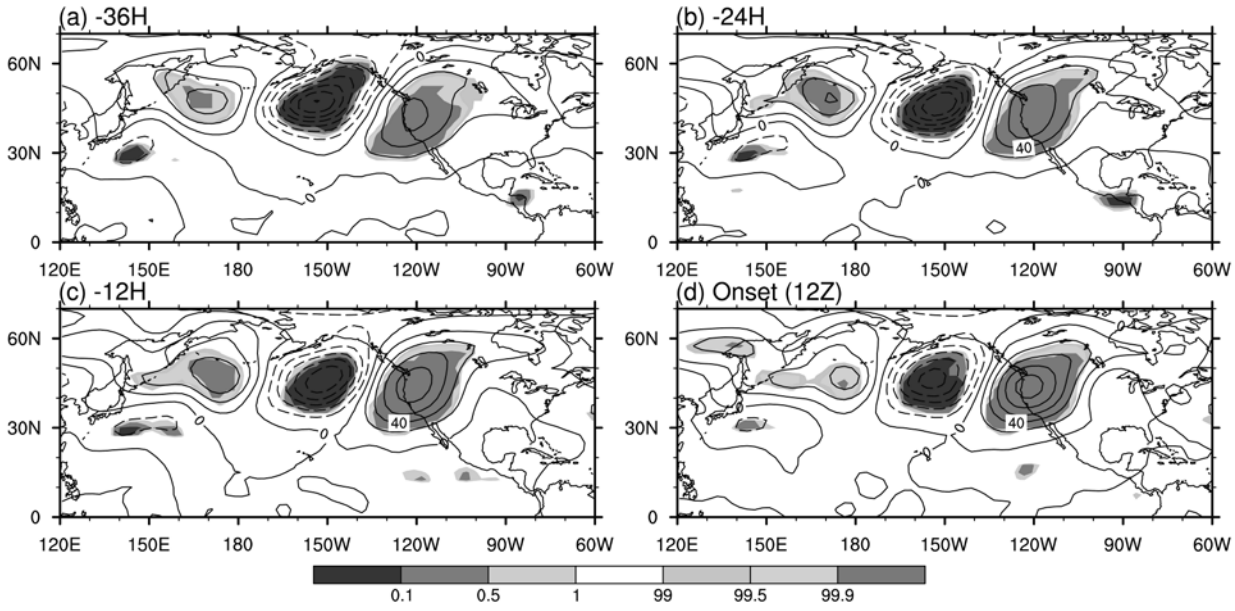

Figure 18.3 LSMP in geopotential height (in m) anomalies at 500 hPa, composites for 49 hot spells target dates from 1951-2010. The target ensemble average from the 12 GMT map immediately prior to each hot spell onset is shown in d). Other panels are at earlier times prior to hot spell onset: a) 36 hours, b) 24 hours, and c) 12 hours. Light shading is used for significant positive anomalies while darker shading is for significant negative anomalies. Scale at the bottom indicates the level of significance in percent compared with 1000 random ensembles.

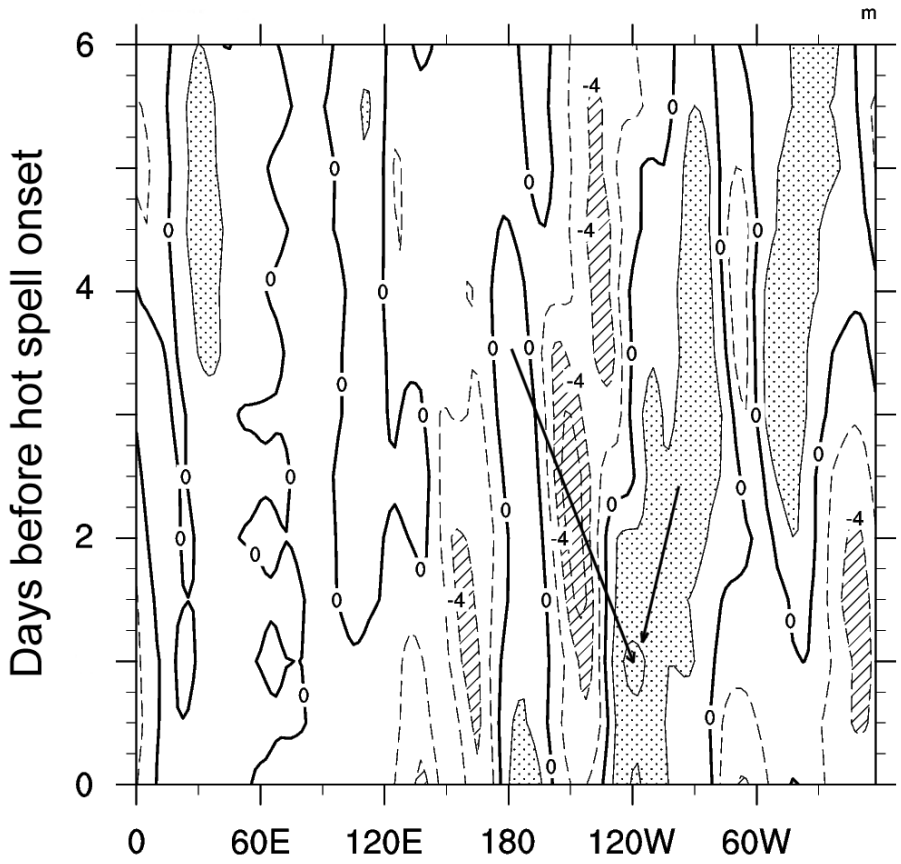

Figure 18.4 Hovmöller diagram of 500 hPa level geopotential height anomaly (in dam) composite for 23 hot spells that occur from 1979-2006. The height anomaly plotted at each longitude is a meridional average from 30N to 50N. The dotted shaded regions are positive (ridge) values and the hatched shaded regions are negative (trough) values. The ridge-trough-ridge structure across the Pacific is visible from the Dateline to 120W. The ridge near the Dateline precedes the downstream trough and ridge over California (left arrow). To the East is some evidence for a positive (ridge) migrating westward (right arrow).

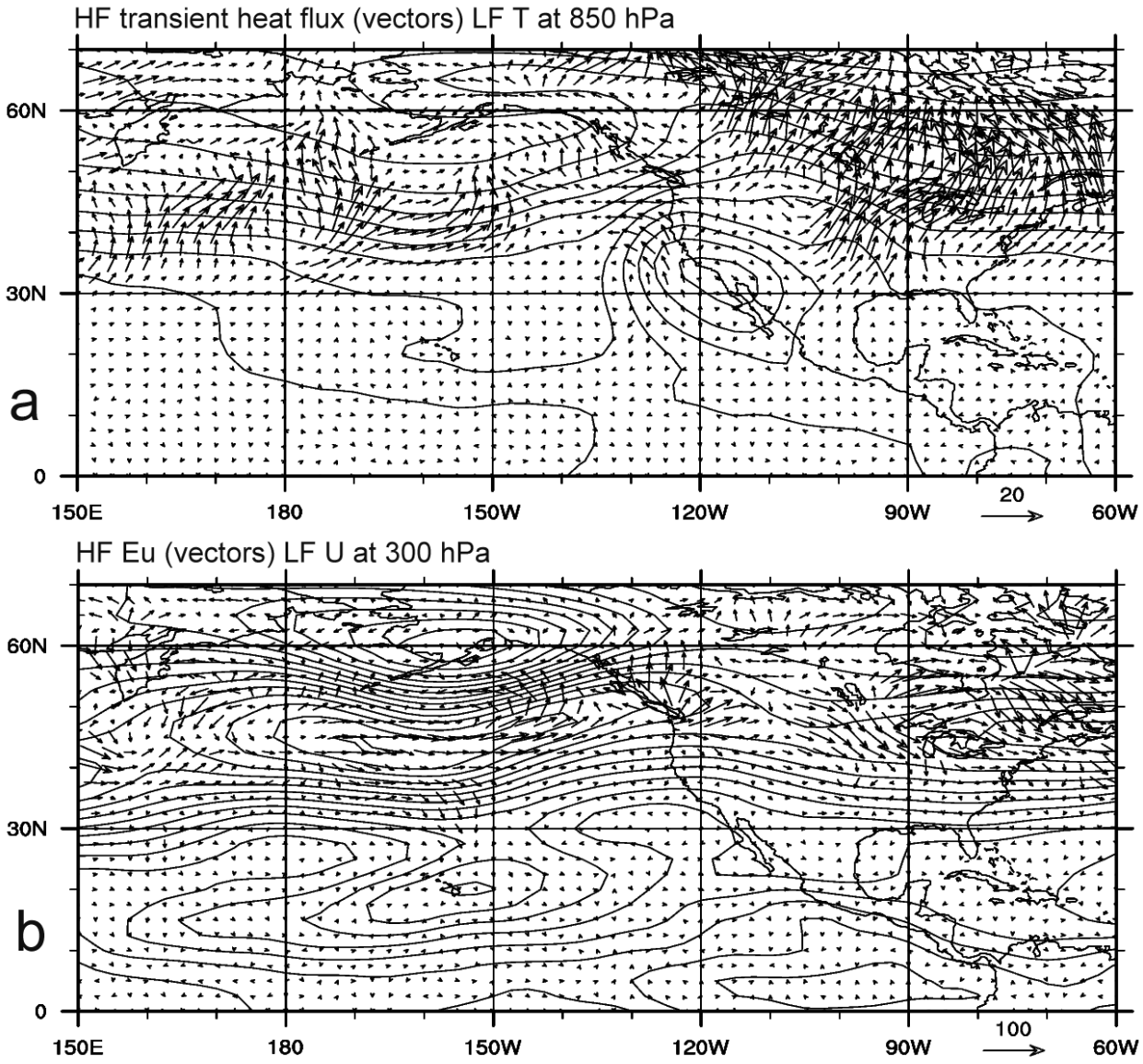

Figure 18.5 Simplified dynamical analysis. a) Horizontal, high frequency (<7 day period), heat flux vectors (mK/s units) superimposed on contours of low frequency temperature (2 K interval) at 850 hPa. These composites are ensemble averages constructed at the onset of 23 hot spell events from 1979-2006. A mass of hot air is migrating out of the southwestern desert region in a direction that keeps the hotter temperatures centered along or off shore of the California coast. b) Horizontal vectors of high frequency E_u (see text; m^2s^{-2} units) and contours of low frequency zonal wind component (2.5 m/s interval). The convergence of E_u reduces the zonal component, consistent with building a ridge along the west coast.

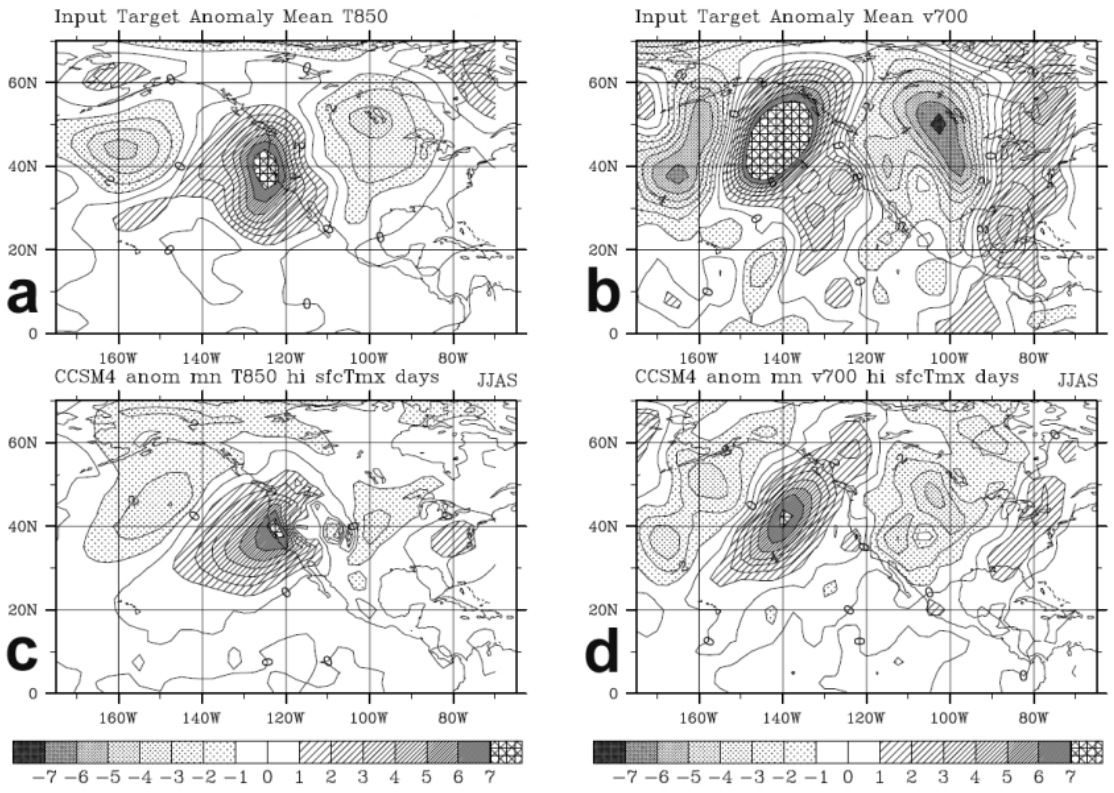

Figure 18.6 Comparison of the reanalysis and climate model LSMPs. Shown are 850 hPa temperature anomaly (K units; left column) and 700 hPa meridional wind (m/s units; right column) in the NDRA2 reanalysis (top row) and in CCSM4 (bottom row) data. The CCSM4 target dates are when values are in the highest 1% average of 3 low elevation, near shore, grid points over land in CCSM4.The model LSMP has a broadly similar LSMP as observed, but some key flaws are: the magnitude is too weak and the 850 hPa maximum temperature anomaly location is onshore instead of offshore.

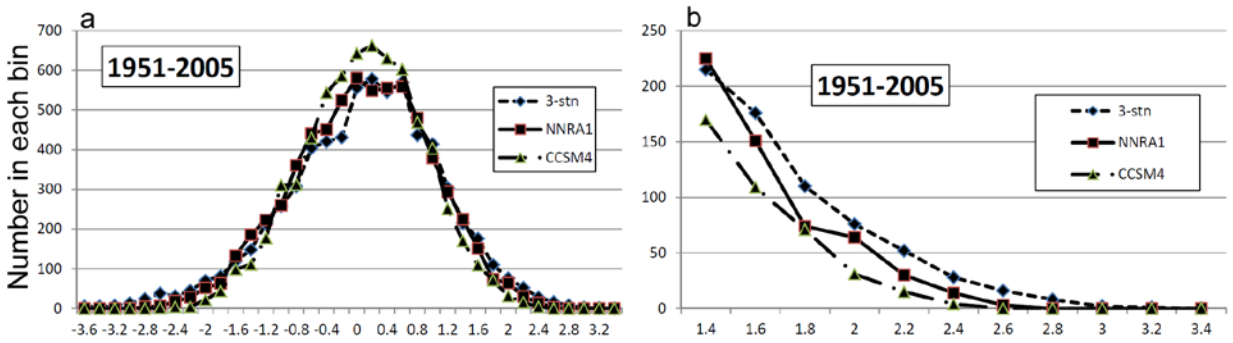

Figure 18.7a) Distribution of LSMP index for NCEP/NCAR reanalysis and CCSM4 data over the period 1951-2005. Also shown are the normalized anomaly average daily values of surface maximum temperature at 3 CV stations over the corresponding period. The overall distributions of reanalysis and surface values match well, even though the index is based only on a few extremely hot events. The distribution of corresponding CCSM4 index values has notably smaller standard deviation. In terms of values above a high threshold, b) the model produces about half as many as occur in the reanalysis data, though the highest index value in the model is comparable to the highest value in the reanalysis. Hence, the model can produce an extreme hot spell, but does so at a rate about half as often as is observed. The horizontal axes are bins of LSMP index values, where the value shown is the lower value of the 0.2 unit range.

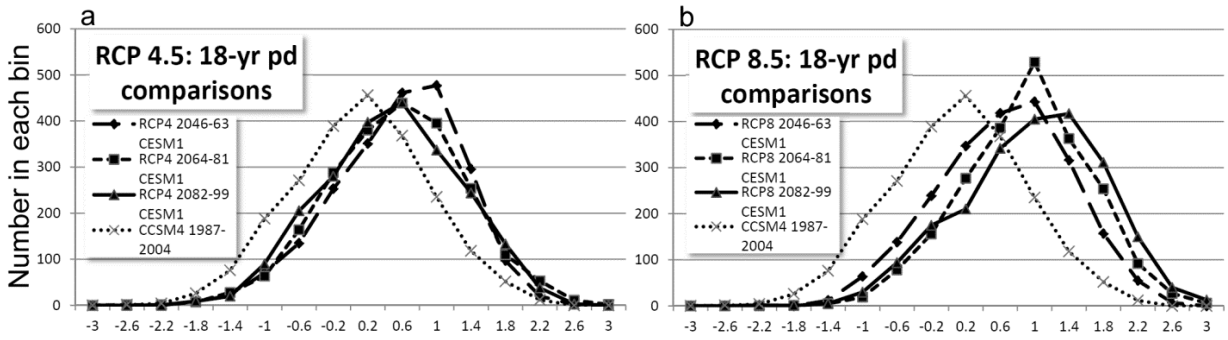

Figure 18.8 Similar to figure 18.7a, except for two representative concentration pathways (RCP) scenarios. CCSM4 LSMP index in 18 year periods a) for RCP 4.5 and b) for RCP 8.5. For reference, the distribution in the model simulation for an 18 year period late in historical simulation is plotted as a dotted line.

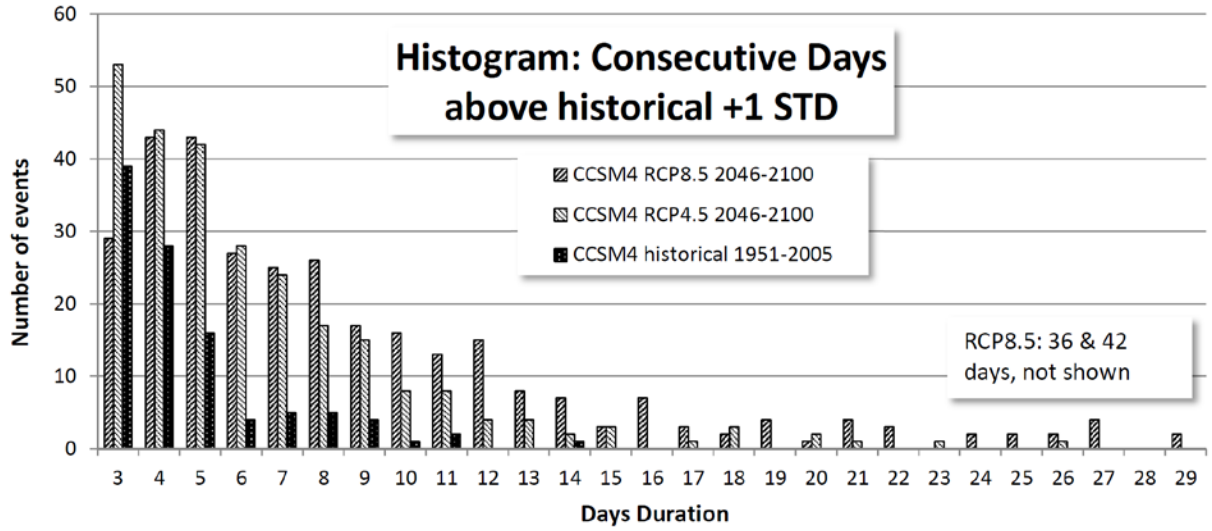

Figure 18.9 Plot of the number of events that CCSM4 LSMP index values exceed 1 standard deviation (based on the historical LSMP distribution) organized by the number of consecutive days the threshold is exceeded during each event. Future climate, RCP scenarios simulated by CCSM4 have more and longer durations above the threshold.

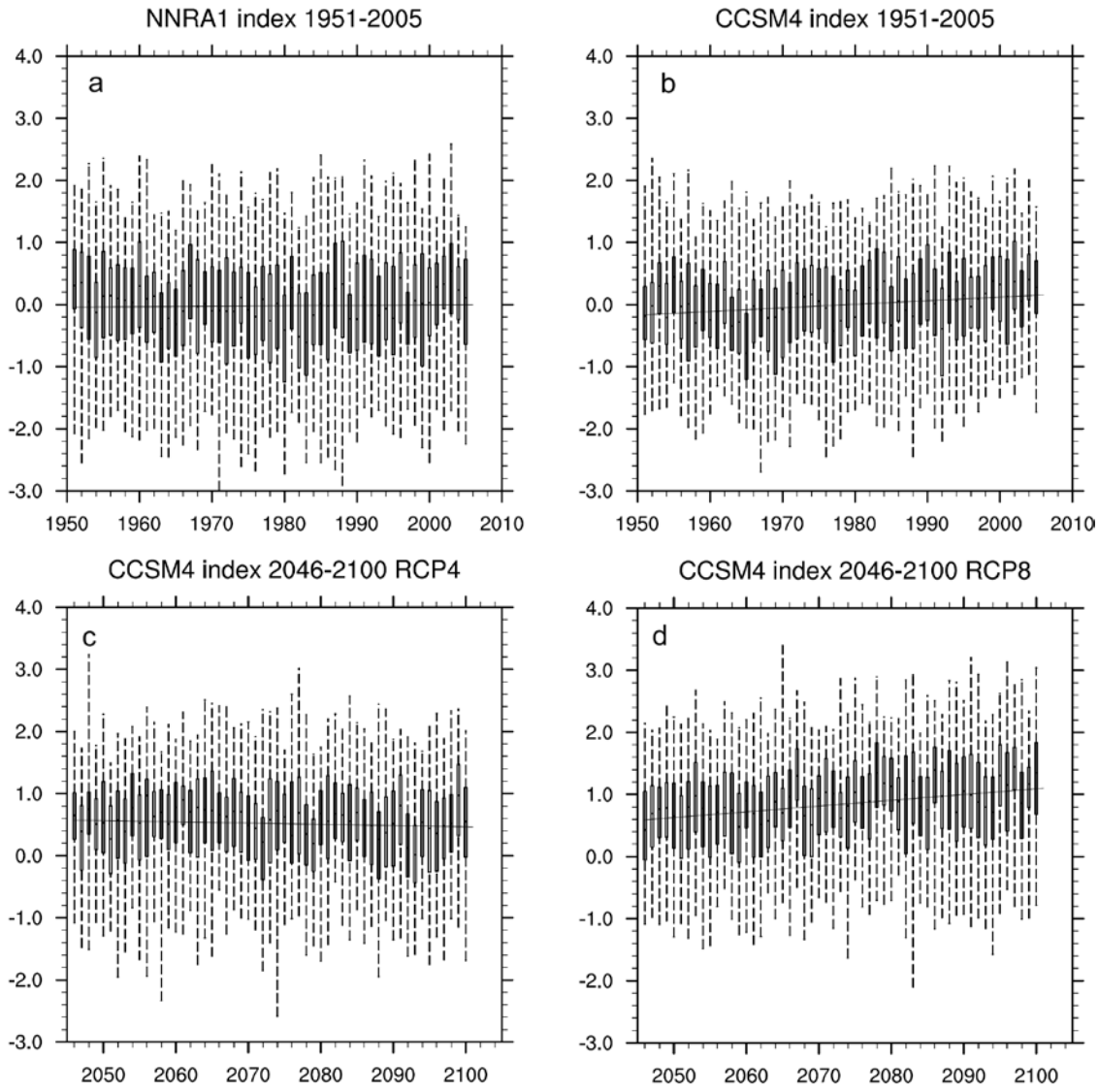

Figure 18.10 LSMP index values from a) NCEP/NCAR reanalysis data (NNRA1) and b) corresponding CCSM4 data from 1951-2005. CCSM4 predictions for 2046-2100 under the c) RCP 4.5 and d) RCP 8.5 emission scenarios. Each box indicates first and third quartiles and the whiskers indicate the extremes in each warm season. Each trend line is calculated using all 55 years of data. In the historical period the model has smaller standard deviation (0.757) than the reanalysis (0.872); also, the model has a larger trend than the reanalysis data. In the two future scenarios, the extreme values are slightly decreasing in the lower emission but strongly increasing in the higher emission scenario. Notably, the standard deviation is essentially unchanged: 0.747 in RCP 4.5 and 0.749 in RCP 8.5. All standard deviations are computed separately for each year then the annual values are averaged together over each 55 year period.

(note: CUP instructions slightly incorrect, index displayed from ‘References’ tab and a choice in the ‘Index’ page.)

Index